Journal of Zhejiang University-SCIENCE A 2026 27(3):275-287
www.jzus.zju.edu.cn; www.springer.com/journal/11582
E-mail: jzus_a@zju.edu.cn

Research Article
https://doi.org/10.1631/jzus.A2500231

Check for updates

Optimization of throttling windows to improve flow control of three-way control combiner valves

Jin-yuan QIAN[1]✉, Zhe-hui MA[1], Shi-jie LIN[1], Chuang LIU[1], Yu-wei WANG[1], Fei LING[2], Liang ZHANG[3], Man-man CUI[3], Tian-zuo QU[4], Zhi-jiang JIN[1]✉

[1]*Institute of Advanced Equipment, Zhejiang University, Hangzhou 310027, China*
[2]*Zhejiang Sanfang Control Valve Co., Ltd., Hangzhou 311400, China*
[3]*Shanghai Nuclear Engineering Research & Design Institute Co., Ltd., Shanghai 200233, China*
[4]*Shandong Nuclear Power Company Ltd., Yantai 265116, China*

Abstract: Three-way control combiner valves (TCCVs) are critical components used in nuclear power plants to regulate the concentration of boron acid for neutron absorption and reactor safety. However, current TCCV designs often suffer from suboptimal control performance and high flow resistance, leading to control deviations and reduced operational efficiency. In this paper, a numerical model based on the standard K–ω turbulence model is established and validated against experimental data to analyze the flow characteristics and local flow resistance of a TCCV. A parametric design method for the throttling windows is proposed, establishing relationships between shape parameters and performance indexes, including control performance and flow resistance. The adaptive non-dominated sorting genetic algorithm (ANSGA-II) is used to optimize the shape parameters of the throttling windows. The optimization results show an improvement in the performance indexes of the TCCV, with the adjustable operating range increasing by 31.0% and the maximum local resistance decreasing by 18.3%. We also introduce the concepts of effective and controllable domains to characterize the inlet backflow phenomena and regulation dead zones, which are crucial for ensuring the reliability and effectiveness of control valves. These findings provide insights for enhancing the design and performance of TCCVs in nuclear power plants.

Key words: Three-way valve; Intersection flow; Throttling windows; Multi-objective optimization

1 Introduction

The demand for clean energy has been increasing globally in recent years (Haneklaus et al., 2023). Therefore, nuclear power is gaining importance due to its low CO_2 emissions (Mallapaty, 2020). Nuclear power plants are essential for meeting this demand while reducing the carbon footprint of energy production (Guo et al., 2024). In nuclear power plants, precise control of boron acid concentration is vital for managing neutron absorption and ensuring reactor safety and stability. Boron acid acts as a neutron poison (Rajesh et al., 2024), and its concentration directly affects the reactor. The three-way control combiner valve (TCCV) plays a vital role in regulating the boron acid concentration by controlling the intersection flow of the boron acid and water. The control performance of TCCVs is essential for preventing both excessive and insufficient reactivity.

Recently, with the rapid development of industry and computer technology, computational fluid dynamics (CFD) has been widely used to study the flow fields inside valves (Qian et al., 2020; Singh et al., 2020; Lin et al., 2021; Chen and Jin, 2023). Control performance (Arbabi Yazdi et al., 2022; Qian et al., 2022; Witrant et al., 2023; Guan et al., 2024) and flow resistance (Ando et al., 2023; Cui et al., 2024) are the key performance indexes. Therefore, numerous studies have investigated these two indexes. Hu et al. (2024) conducted CFD simulations to improve flow control performance, providing 20%–30% more ventilation

✉ Jin-yuan QIAN, qianjy@zju.edu.cn
Zhi-jiang JIN, jinzhijiang@zju.edu.cn
Jin-yuan QIAN, https://orcid.org/0000-0002-5438-0833
Zhi-jiang JIN, https://orcid.org/0000-0002-8063-709X

Received June 4, 2025; Revision accepted Aug. 19, 2025;
Crosschecked Jan. 11, 2026; Online first Feb. 6, 2026

in the forward direction and 10%–15% less in the reverse direction than before, aiming to enhance indoor air quality. Vašina et al. (2015) dealt with an investigation of the dynamic behavior of a three-way throttle valve, ensuring its control performance in maintaining constant flow despite load changes. Hopfgartner et al. (2022) investigated a force-assisted suction valve in hermetic reciprocating compressors, using an electromagnetically actuated spring to reduce flow resistance, thereby improving reliability and reducing noise. Hadebe et al. (2024) highlighted the effective control performance and reduced flow resistance of a multi-door check valve, demonstrating improvements in backflow prevention and pressure drop. Blasiak et al. (2021) designed a pneumatic directional control valve using rapid prototyping and CFD simulations, achieving high flow rates and low flow resistance, which enables more efficient and responsive air direction control.

To enhance the performance of a TCCV, it is necessary to optimize its structure. Some scholars have attempted to design new structures to improve the performance of valves. Regression fitting and optimization algorithms have been proven to be applicable to the structural optimization of valves (Gui et al., 2022; Zong et al., 2022a; Zhao et al., 2023). Filho et al. (2023) designed a new hydraulic valve model to improve control performance and reduce flow resistance by optimizing the valve's geometry, resulting in a decrease in the pressure drop coefficient and enhanced controllability. Kang et al. (2024) optimized the lengths of the waist and tail regions of the bottom plug in a three-way valve, reducing the local cavitation percentage (POC) from 34.90% to 15.84%. Yang et al. (2023) used a surrogate model-based optimization approach to reduce the pressure drop and improve the control performance of multi-way spool valves using K-shaped notches. This optimization resulted in a 7.23% reduction in average pressure drop and a 1.28% flow area relative deviation. Filo et al. (2021) optimized the geometry of the flow channels and holes inside a check valve based on the results of a CFD simulation, resulting in a 40% reduction in pressure loss. Zong et al. (2022b) developed an ensemble surrogate model to optimize steam safety valves, reducing the minimum blowdown from 13.30% to 2.70%. Lisowski et al. (2023) proposed a new three-way valve design with two circumferentially distributed outlets. This design maintains a required flow rate with supply pressure only slightly above the loading pressure, significantly reducing the energy losses. Further work (Lisowski et al., 2024) was done to limit the maximum flow rate non-uniformity to 6.3% by optimizing the spool geometry and spring parameters. Wang et al. (2024) used radial basis function (RBF) neural networks and multi-island genetic algorithms (MIGAs) to optimize the throat structure parameters of a hydraulic throttle valve, effectively reducing the valve's noise. Bao and Wang (2022) proposed a novel Tesla valve with a special tapering/widening structure, demonstrating a superior absolute pressure drop ratio. The design achieved a maximum temperature difference of 12.10 K between forward and reverse flows, enhancing its potential for real-time thermal management. Brilianto et al. (2020) redesigned damping holes to prevent the hunting phenomenon, suppressing vibration and noise while maintaining the mass flow rate.

Although numerous studies have investigated the design and optimization of valves, they have had several limitations. Most studies focus either on control performance or flow resistance, but rarely both together. In addition, lots of studies concentrate on two-way valves, which have only one inlet and one outlet. However, recent studies have revealed specific limitations of three-way valves because of the complexity of their channels and intersection flow. Even when such valves are studied, the different numbers and locations of inlets and outlets can lead to operating conditions significantly different from those resulting from using the TCCV described in this paper.

To address these limitations, we propose a numerical model of a TCCV used in nuclear power plants and validate its accuracy using an experimental platform. A calculation method for flow rate under various operating conditions has been developed based on the principle of intersecting flow. Furthermore, based on this method and the analysis of the inlet backflow phenomenon, two performance indexes for evaluating the control performance and flow resistance of TCCVs are proposed. A parametric design method and adaptive non-dominated sorting genetic algorithm (ANSGA-II) are used to optimize the shape of the throttling window in the TCCV to improve the performance indexes.

2 Methodology

2.1 Physical model and numerical method

The TCCV (Fig. 1a) has two inlets and an outlet. There are four rectangular throttling windows on the sleeve, distributed in the circumferential direction. During operation, a mixture of 4375 mg/L boric acid and water enters the valve chamber from inlet 1. Desalted water enters from inlet 2. After the two fluids converge in the valve chamber, the mixture with the lower boric acid concentration flows out from the outlet. When the valve core moves from top to bottom, the flow rate of inlet 2 decreases, while the flow rate of inlet 1 increases. The parameters of the TCCV are shown in Table 1. The diameters of the outlet and the two inlets are all 80 mm.

CFD analysis requires a discrete channel model. Therefore, the fluid domain of the valve was discretized into grid elements (Fig. 1b). To ensure the flow is fully developed, both the inlet and outlet channels were extended.

The quality of the grid is vital for the accuracy of the numerical result. We used the grid convergence index to evaluate the mesh quality. The grid convergence index $G_{i+1,i}$ (i is the sequence number of the grid, and i=1, 2, 3) was calculated as follows:

$$G_{i+1,i}=F_{\mathrm{s}}\frac{e_{i+1,i}}{r-1}, \tag{1}$$

where F_{s} is the grid refinement coefficient and is set as 1.25; r is the grid refinement factor and is set as 1.5; $e_{i+1,i}$ is the relative error. The acceptable limits for both $e_{i+1,i}$ and $G_{i+1,i}$ are set as 5%.

When conducting CFD simulations, water at room temperature was used as the fluid, because in the operating conditions of this study, the mass ratio of boric acid to water was below 5%. Boric acid has little effect on the physical properties of the fluid. Meanwhile, the physical properties of water at 66 °C are not significantly different from those at room temperature.

After calculating convergence, the convergence accuracy A, flow rate Q, relative error $e_{i+1,i}$, and the grid convergence index $G_{i+1,i}$ were obtained (Table 2). The maximum relative error and grid convergence index of the second grid were 3.35% and 4.22%, respectively, and both were below the acceptable limit. The second grid with mesh number N_{grids}=18.20×10^5 was chosen for this study based on its computational efficiency and accuracy.

To conduct CFD analysis, selecting a suitable grid model is essential. Several turbulence models are commonly used to simulate the operating conditions of a TCCV, including the standard K–ε, realizable K–ε, standard K–ω, and shear stress transport (SST) K–ω models (K, ε, and ω are the turbulent kinetic energy, turbulent dissipation rate, and specific dissipation rate, respectively). To identify the most suitable turbulence model, the simulation results of four turbulence models were compared with experimental results (Fig. 2). In the simulation, the pressure of inlet 1 and inlet 2 was 100 kPa. The x-axis represents the degree of opening of the TCCV N_{l}, and the y-axis represents the flow coefficients of B to A and C to A. The simulation results of the standard K–ω model had the smallest average deviation from the experimental results (4.5%), so this model was chosen for this study.

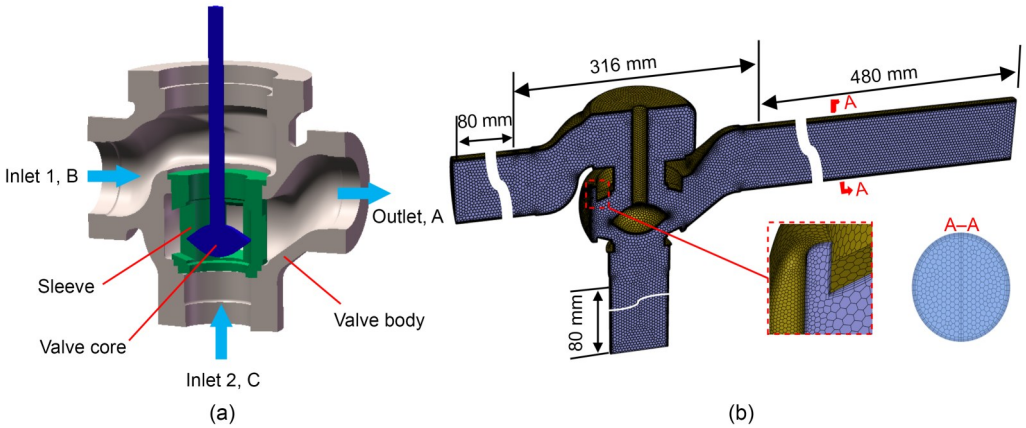

Fig. 1 Geometry and grid of the TCCV: (a) geometry; (b) grid of fluid domain. A–A is the grid of the outlet cross-section

Table 1 Parameters of the TCCV

Parameter	Value
Inlet pressure (kPa)	90
Design temperature (°C)	66
Rated flow coefficient from B to A, $C_{B\to A}$	60
Rated flow coefficient from C to A, $C_{C\to A}$	80
Caliber (mm)	80.0
Stroke (mm)	49.8
Opening response time (s)	55.00
Closing response time (s)	57.90

Table 2 Grid convergence indexes

i	N_{grids} ($\times10^5$)	Q (kg/s)	A	$e_{i+1,i}$ (%)	$G_{i+1,i}$ (%)
1	5.72	2.651	1.92	–	–
2	18.20	2.743	1.92	3.35	4.22
3	60.10	2.760	1.92	0.68	2.98

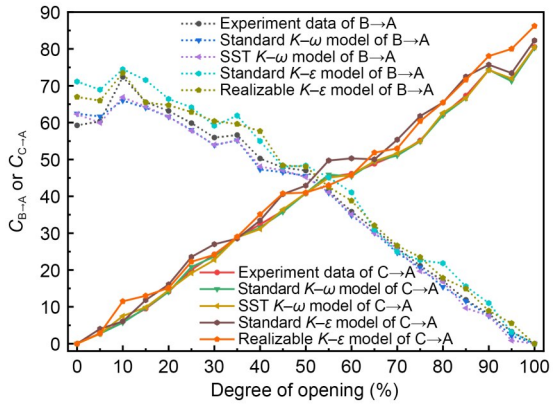

Fig. 2 Comparison between the results of the four turbulence models and the experimental results

2.2 Mathematics method

The shape of the throttle window has a significant impact on the performance of a TCCV, especially its control performance and flow resistance. A parametric design method is proposed to optimize the shape of the throttling window. As shown in Fig. 3a, the length x of the throttling window in the X-direction is equal to the stroke of the valve L_{max}, while the width of the throttling window in the Y-direction is determined by the function $f_w(x)$. The coordinate origin O of the XOY coordinate system is the midpoint of the lower boundary of the throttling window. The Y-axis direction is the width direction of the throttling window, corresponding to the circumferential direction of the sleeve. The X-axis direction is the length direction of the throttling window, corresponding to the axial

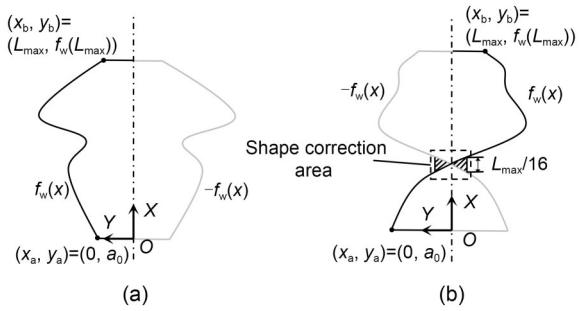

Fig. 3 Parametric design method for throttling window: (a) non-zero-crossing case; (b) zero-crossing case

direction of the sleeve. To prevent erosion caused by a narrow width, the minimum length in the X-direction was set to 1/16 of the valve stroke. As shown in Fig. 3b, when the function $f_w(x)$ crosses the X-axis, the area at the narrowest area is corrected. x_a=0 and y_a=a_0 are the x-coordinate and y-coordinate of the starting point of $f_w(x)$, respectively; x_b=L_{max} and y_b=$f_w(L_{max})$ are the x-coordinate and y-coordinate of the end point of $f_w(x)$, respectively.

In this study, we chose the polynomial function $f_w(x)$ as the function that determines the width of the throttling window because the polynomial function has flexible shapes, and there are no breakpoints or infinite problems. Due to limitations in computational capacity, $f_w(x)$ was selected as a cubic polynomial.

To guide the optimization of the design of the throttling windows, a method for calculating the intersection flow is proposed (Fig. 4). The pressure difference of the two inlets ΔP, outlet flow rate Q_o, and degree of opening N_l correspond one-to-one.

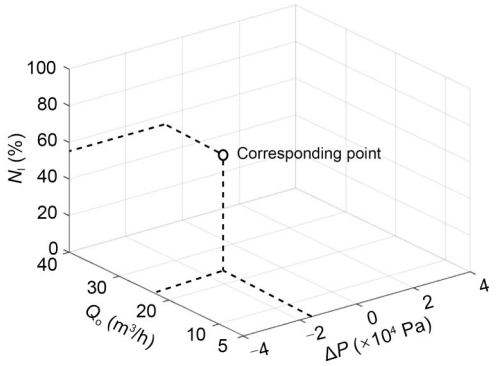

Fig. 4 Schematic diagram of the intersecting flow calculation method

For any throttling window inside the TCCV, according to the Bernoulli equation:

$$\frac{P_1}{\rho g}+\frac{\alpha_1 Q_1^2}{2gA_{\text{in}}^2}=\frac{P_{\text{o}}}{\rho g}+\frac{\alpha_{\text{o}} Q_{\text{o}}^2}{2gA_1^2}+h_{\text{fl}}, \tag{2}$$

where P_1 and P_{o} are the pressures of inlet 1 and outlet, respectively; ρ is the density of the fluid; g is the gravitational acceleration; α_1 and α_{o} are the kinetic energy correction factors of inlet 1 and outlet, respectively; Q_1 and Q_{o} are the flow rates of the throttling window on the side of inlet 1 and outlet, respectively; A_{in} is the equivalent inlet area of the throttling window; A_1 is the throttling area on the side of inlet 1; h_{fl} is the head loss on the side of inlet 1. Specifically, the total flow rate at the inlet will be unevenly allocated to the four throttling windows. According to the principle of flow rate allocation, the equivalent inlet area A_{in} can be calculated.

The head loss h_{f} can be calculated by the method proposed by Guan et al. (2023). Then, outlet pressure P_{o} can be calculated:

$$P_{\text{o}}=(1-\xi_1)\frac{\alpha_1\rho Q_1^2}{2A_{\text{in}}^2}-\frac{\alpha_{\text{o}}\rho Q_1^2}{2R_1^2A_{\text{in}}^2}+P_1, \tag{3}$$

where ξ_1 is the local flow resistance coefficient at the throttling window on the inlet 1 side; R_1 is the equivalent contraction ratio of A_1 to A_{in}.

Similarly, a corresponding formula holds for inlet 2. Obviously, as TCCV has only one outlet, the outlet pressure of the inlet 1 side is equal to the outlet pressure of the inlet 2 side. In this study, the areas of the two inlets were the same. Thus, the following equation can be derived:

$$\frac{Q_1}{Q_2}=\frac{R_1\sqrt{(1+\xi_2R_2^2-R_2^2)(P_1-P_{\text{o}})}}{R_2\sqrt{(1+\xi_1R_1^2-R_1^2)(P_2-P_{\text{o}})}}, \tag{4}$$

where Q_2 is the flow rate of the inlet 2; R_2 is the equivalent contraction ratio of A_2 to A_{in}, and A_2 is the throttling area on the side of inlet 2; ξ_2 is the local flow resistance coefficient at the throttling window on the inlet 2 side; P_2 is the pressure of inlet 2.

Therefore, the flow rates of the upper and lower sides of the throttling window, which are separated by the valve core, exhibit a ratio determined by the degree of opening and the pressure difference at the two inlets. When the TCCV is in operation, the outlet flow rate Q_{o} of the throttling window is:

$$Q_{\text{o}}=Q_1+Q_2, \tag{5}$$

$$\frac{R_1}{\sqrt{R_1^4-2R_1^3+1}}\sqrt{P_1-P_{\text{o}}}+\frac{R_2}{\sqrt{R_2^4-2R_2^3+1}}\sqrt{P_2-P_{\text{o}}}=\frac{Q_{\text{o}}}{A_{\text{in}}}\sqrt{\frac{\rho}{2}}. \tag{6}$$

Thus, when any two out of the three parameters (ΔP, Q_{o}, and N_{l}) are known, the value of the third parameter can be obtained from Eq. (6). In specific calculations, we use ΔP and N_{l} to obtain Q_{o}. When the Q_{o} values of the four throttling windows are known, the flow rates of inlet 1 and inlet 2 (Q_1 and Q_2) can be gained from Eq. (4).

2.3 Experimental platform

To obtain the flow characteristics of the TCCV and validate the numerical model, we conducted flow testing experiments on the valve. The experimental platform is shown in Fig. 5. In addition to the TCCV under test, the experimental platform components include a buffer tank, a surge tank, a manual ball valve, a pressure relief valve (PRV), a manual globe valve, pressure gauges, piping and pipe supports, and an electronic display screen.

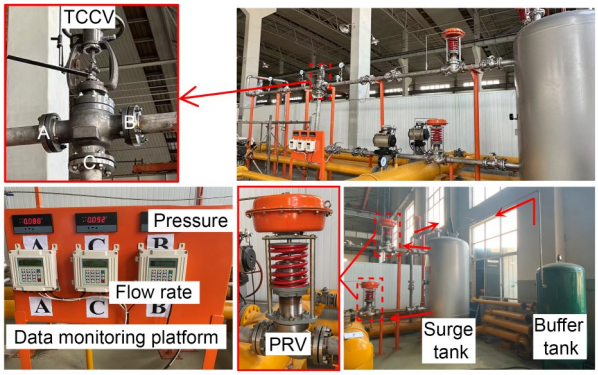

Fig. 5 Experimental platform

The inlets of the TCCV were connected to a surge tank, which ensured the stability of the inlet pressure. The flow rate was regulated through a manual control valve on the outlet pipeline. In the experiment, the degree of opening of the TCCV was adjusted, and the pressures and flow rates in each branch were measured at different degrees of valve opening. Then, the flow coefficient was calculated.

2.4 Fitting and optimization

The ANSGA-II used in this study is based on the regression fitting shown in Fig. 6. The overall process includes initial population generation, crossover and mutation iteration, quadratic regression fitting, and output of the optimal solution.

First, to conduct the genetic algorithm, we use quadratic regression fitting to establish the relationship between independent variables (design parameters) and dependent variables (optimization objective).

For the crossover and mutation iteration part, an initial population first needs to be randomly generated. The initial population size was 200, and the number of iterations was 300. The design parameters of the initial 200 individuals were randomly generated within the design space, and their fitness functions were calculated based on the regression fit results. Then, adaptive crossover and mutation occur in the population to produce the next generation.

This adaptiveness means that the crossover and mutation probability of each individual in the population dynamically changes according to its fitness function. The crossover and mutation probabilities p_c and p_m of each individual in the population are:

$$p_c=\begin{cases}p_{c1}-\dfrac{(p_{c1}-p_{c2})(f_c-f_{ave})}{f_{max}-f_{ave}}, & f_c>f_{ave},\\ p_{c1}, & f_c\leqslant f_{ave},\end{cases}$$
$$p_m=\begin{cases}p_{m1}-\dfrac{(p_{m1}-p_{m2})(f_m-f_{ave})}{f_{max}-f_{ave}}, & f_m>f_{ave},\\ p_{m1}, & f_m\leqslant f_{ave},\end{cases} \tag{7}$$

where f_c and f_m are the total fitness function values of the individual participating in crossover and mutation, respectively; f_{ave} is the average of all the fitness function values in this generation; f_{max} is the maximum of all the fitness function values in this generation; p_{c1}=0.8, p_{c2}=0.6, p_{m1}=0.2, and p_{m2}=0.1 are the upper and lower limits of crossover and mutation probabilities.

After the crossover and mutation part, the number of individuals in the population increases. At this point, it is necessary to eliminate bad individuals from the population for further optimization. The main processes involved in elimination include non-dominated sorting and crowding distance calculation.

Then, ecological ranks among individuals in the population are established based on the Pareto principle. In non-dominated sorting, each individual in the population is compared with every other to determine dominance relationships and ecological ranks. When

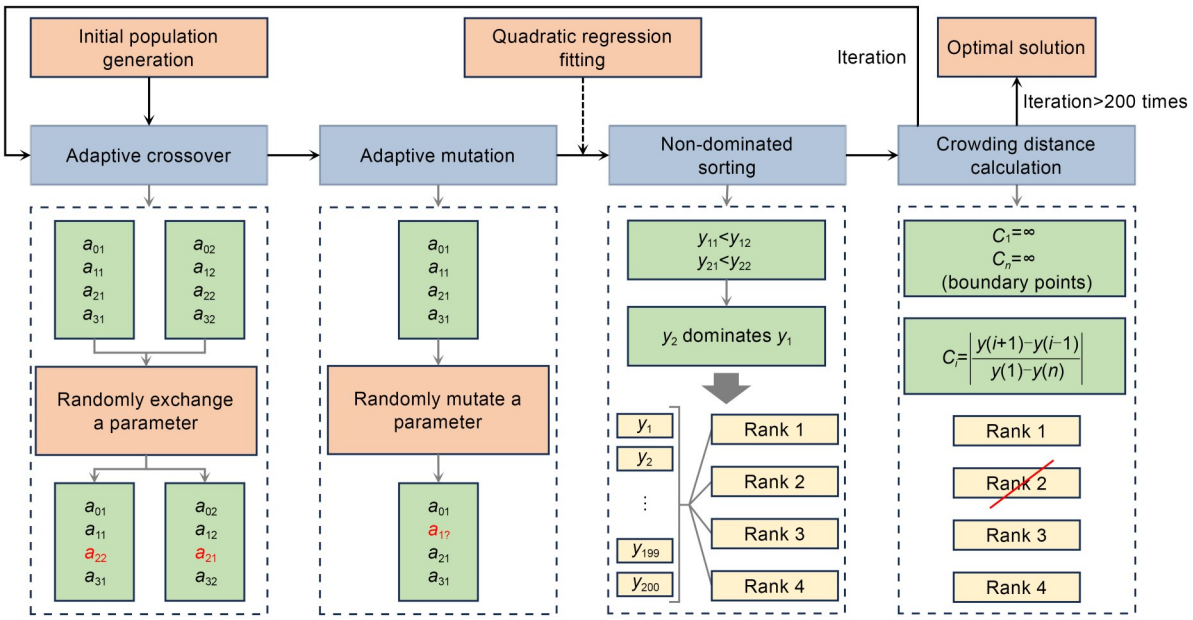

Fig. 6 Block diagram of ANSGA-II. a_{i1} and a_{i2} (i=0, 1, 2, 3) are the polynomial coefficients; $a_{1?}$ is the polynomial coefficient randomly chosen for mutation; y_{11}, y_{12}, y_{21}, and y_{22} are the optimization objectives calculated by functions obtained from quadratic regression fitting; y_i (i=1, 2, ⋯, 200) is the individual in the population; $y(i)$ (i=1, 2, ⋯, n) is the fitness function value; C_i (i=1, 2, ⋯, n) is the crowding distance; n is the number of individuals in the rank

the number of iterations is large enough, every individual in the population has a high fitness function, and no dominance relationship can be established among them.

After completing non-dominated sorting, the crowding distance of each rank needs to be calculated. This is because individuals within each rank cannot establish dominance relationships, making it impossible to determine which individual will be eliminated during elimination. When calculating the crowding distance C_i, individuals at the ecological rank are first sorted according to their fitness function values, and then C_i is calculated using the following formula:

$$C_i=\begin{cases}\infty, & i=1,\\ \left|\dfrac{y(i+1)-y(i-1)}{y(1)-y(n)}\right|, & i=2,\ 3,\ \cdots,\ n-1,\\ \infty, & i=n.\end{cases} \quad (8)$$

Calculating the crowding distance retains boundary individuals in the iteration and eliminates concentrated individuals, maintaining diversity in the population and preventing local optima. After non-dominated sorting and crowding distance calculation, the population undergoes elimination, leaving 200 individuals, the same as the initial population size. These individuals repeat the previous crossover and mutation iteration processes, cycling 300 times. Finally, in the Pareto front, multiple fitness functions are balanced to obtain the optimal solution in the design space.

3 Results and discussion

The results are presented in three sections. Firstly, the flow rate ratio for each throttling window was simulated and analyzed. Subsequently, the velocity v distribution on the symmetry plane of the flow field within the TCCV was analyzed under different inlet pressure conditions to investigate the backflow phenomenon. Finally, ANSGA-II was applied to optimize the shape of the throttling window to enhance the control performance of the TCCV while reducing the flow resistance.

3.1 Flow rate ratio of throttling windows

Based on the method proposed in Section 2.2 for calculating the intersection flow, the flow rate of the TCCV can be calculated. However, if the allocation of flow rate for each throttling window is unknown, the equivalent inlet area A_{in} and equivalent contraction ratio R are also difficult to obtain. That means it is necessary to conduct numerical simulations to obtain the percentage of flow rate Q_i (i represents R, m1, m2, or L) for each throttling window. The Q_i values under different degrees of opening N_I obtained from simulation are presented in Fig. 7. Q_R is the Q_i of the right throttling window, Q_{m1} and Q_{m2} are the Q_i of the two middle throttling windows, and Q_L is the Q_i of the left throttling window.

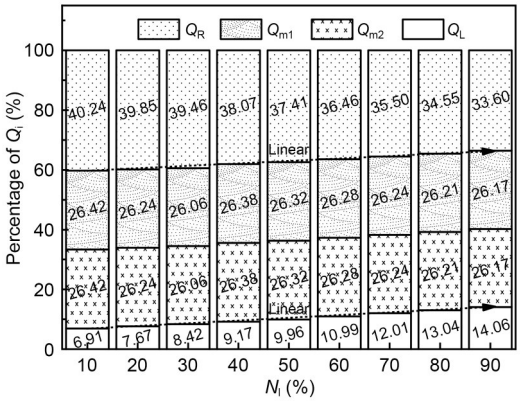

Fig. 7 Percentage of flow rate Q_i allocation under different degrees of opening N_I

Fig. 7 shows that when the degree of opening N_I changes, the Q_i of the two middle throttling windows hardly changes, with the maximum relative change not exceeding 5%. This indicates that if the outlet flow rate and inlet pressure remain unchanged, the flow rate percentages of the two middle throttling windows tend to be constant when the degree of opening N_I changes. Secondly, due to the different distances between each throttling window and the outlet pipeline, their Q_i is not uniform. The Q_i of the right throttling window is the highest, and the Q_i of the left throttling window is the lowest.

Note that as N_I increases, Q_R gradually decreases, showing an approximately linear trend. In contrast, Q_L gradually increases but also shows a linear trend. From the perspective of flow resistance, this is because the flow resistance of the inlet 1 side channel is greater than that of the inlet 2 side channel. When N_I= 50%, according to the analysis in the previous section, due to the corner of the flow channel on the inlet 1 side, the velocity at inlet 2 is greater than that at inlet 1.

Therefore, there are two main flow resistances for fluid flowing from the inlet to the outlet of the throttling windows: the inlet channel and the throttling window. For the inlet 1 side, the flow resistance of the inlet channel is relatively large, and the flow resistance of the throttling window is relatively small, so the flow distribution is more uniform. For the inlet 2 side, the flow resistance of the inlet channel is relatively small, and the flow resistance of the throttling window is large, resulting in an uneven allocation of flow rate. Therefore, when N_l is small, the flow rate of the right throttling window is much greater than that of the left window, and when N_l increases, the flow rates on both sides begin to approach each other.

Subsequently, to obtain the equivalent contraction ratio R of each throttling window, Q_i needs to be fitted as follows:

$$Q_\mathrm{R}=0.410-0.83N_\mathrm{l}, \tag{9}$$

$$Q_\mathrm{L}=0.064+0.83N_\mathrm{l}, \tag{10}$$

$$Q_\mathrm{m1}=Q_\mathrm{m2}=26.3\%. \tag{11}$$

As the fitting error is within 2%, it can be considered that the empirical formula is accurate. Then, R can be calculated as follows:

$$R_\mathrm{i,1}=k\frac{1-N_\mathrm{l}}{Q_\mathrm{i}}, \tag{12}$$

$$R_\mathrm{i,2}=k\frac{N_\mathrm{l}}{Q_\mathrm{i}}, \tag{13}$$

where $R_\mathrm{i,1}$ and $R_\mathrm{i,2}$ (i represents R, m1, m2, or L) are the equivalent contraction ratios R of the corresponding throttling window on the inlet 1 side and inlet 2 side, respectively; k is the ratio of the throttling window area to the inlet area. The above equation applies only to rectangular throttling windows. For throttling windows with parametric contours, k can be calculated using the following equation:

$$k=\frac{2\int_0^{L_\mathrm{max}}|f_\mathrm{w}(x)|\mathrm{d}x}{A_\mathrm{in}}. \tag{14}$$

Then, R can be calculated as follows:

$$R_\mathrm{i,1}=\frac{2\int_0^{L_\mathrm{max}}|f_\mathrm{w}(x)|\mathrm{d}x-2\int_0^{N_\mathrm{l}L_\mathrm{max}}|f_\mathrm{w}(x)|\mathrm{d}x}{\frac{\pi}{4}D^2Q_\mathrm{i}}, \tag{15}$$

$$R_\mathrm{i,2}=\frac{2\int_0^{N_\mathrm{l}L_\mathrm{max}}|f_\mathrm{w}(x)|\mathrm{d}x}{\frac{\pi}{4}D^2Q_\mathrm{i}}, \tag{16}$$

where D is the diameter of the two inlets.

In summary, R can be calculated using N_l and Q_i, and the performance indexes of the TCCV can be calculated when the pressure difference of two inlets ΔP is known.

3.2 Backflow analysis

When the pressure of the two inlets is unequal, there may be inlet backflow in the TCCV. In practical engineering applications, backflow can cause problems such as internal leakage, overpressure, and incorrect outlet medium concentration. Thus, this phenomenon needs to be analyzed and prevented. The inlet backflow at the degree of opening of 50% is shown in Fig. 8. The emergence and development of the inlet backflow phenomenon can be divided into four stages. First, when ΔP=0 (Fig. 8a), the velocity of inlet 2 is larger than that of inlet 1 because of the corner on the main channel of the inlet 1 side. Second, the pressure at inlet 1 is 5 kPa higher than that at inlet 2 (Fig. 8b). The velocity at inlet 2 decreases, but the overall flow situation shows no significant changes compared with the first stage. In the third stage, the inlet pressure difference ΔP in this situation is 10 kPa (Fig. 8c). The velocity at inlet 2 further decreases, approaching 0.

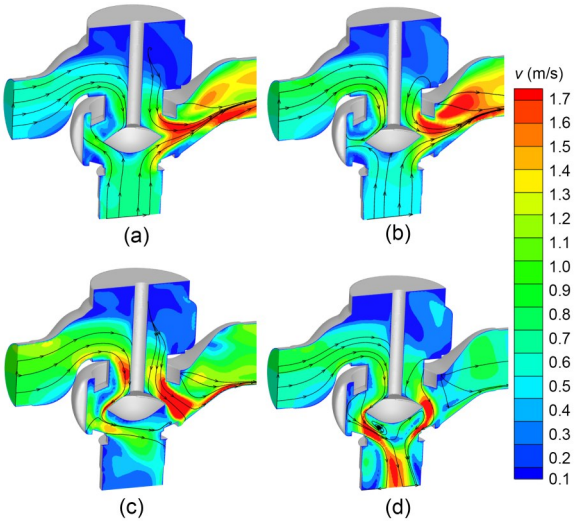

Fig. 8 Inlet backflow phenomenon in the TCCV under different pressure conditions: (a) ΔP=0 kPa; (b) ΔP=5 kPa; (c) ΔP=10 kPa; (d) ΔP=30 kPa

There is only one pathway inside the valve, from inlet 1 to the outlet. Finally, ΔP increases to 30 kPa (Fig. 8d). The flow velocity at inlet 2 increases, but the flow direction is opposite to that of the first stage. There are two pathways inside the valve, namely from inlet 1 to inlet 2 and to the outlet, respectively. In this situation, the phenomenon of inlet backflow is very obvious. The flow rate at inlet 2 is higher than that at the outlet because when the fluid flows out from inlet 2, it does not need to change its direction greatly.

During the operation of the TCCV, it is necessary to avoid inlet backflow as much as possible. When inlet backflow occurs, the TCCV is unable to control the concentration of boric acid at the outlet. So, the TCCV is effective only when there is no inlet backflow. Based on the analysis of the flow field, due to the maximum resistance in the left throttling window, the backflow problem first occurs in this window. Therefore, as long as there is no backflow in the left throttling window, it can be determined that the valve is effective. The flow rate of the left throttling window can be calculated by the method for intersection flow characteristics proposed in Section 2.2. When the calculated flow rate of any inlet is 0, there is backflow in the valve, and the valve is ineffective. The effective boundary is shown in Figs. 9a and 9b.

In addition to preventing backflow, the control performance of the TCCV is also important. In this study, we used the derivative of the inlet flow ratio for the degree of opening N_1 as an index to measure the control performance:

$$N_a = \left| \lim_{N_1 \to 0} \frac{K_q(N_1 + \Delta N_1) - K_q(N_1)}{\Delta N_1} \right|, \qquad (17)$$

where N_a is the control performance index; K_q is the ratio of inlet flow rate to outlet flow rate. To ensure that the evaluation of control performance is not affected by dimensions, K_q was chosen as the value for calculating N_a.

The operating condition with a control performance index N_a<0.3 is defined as an uncontrollable

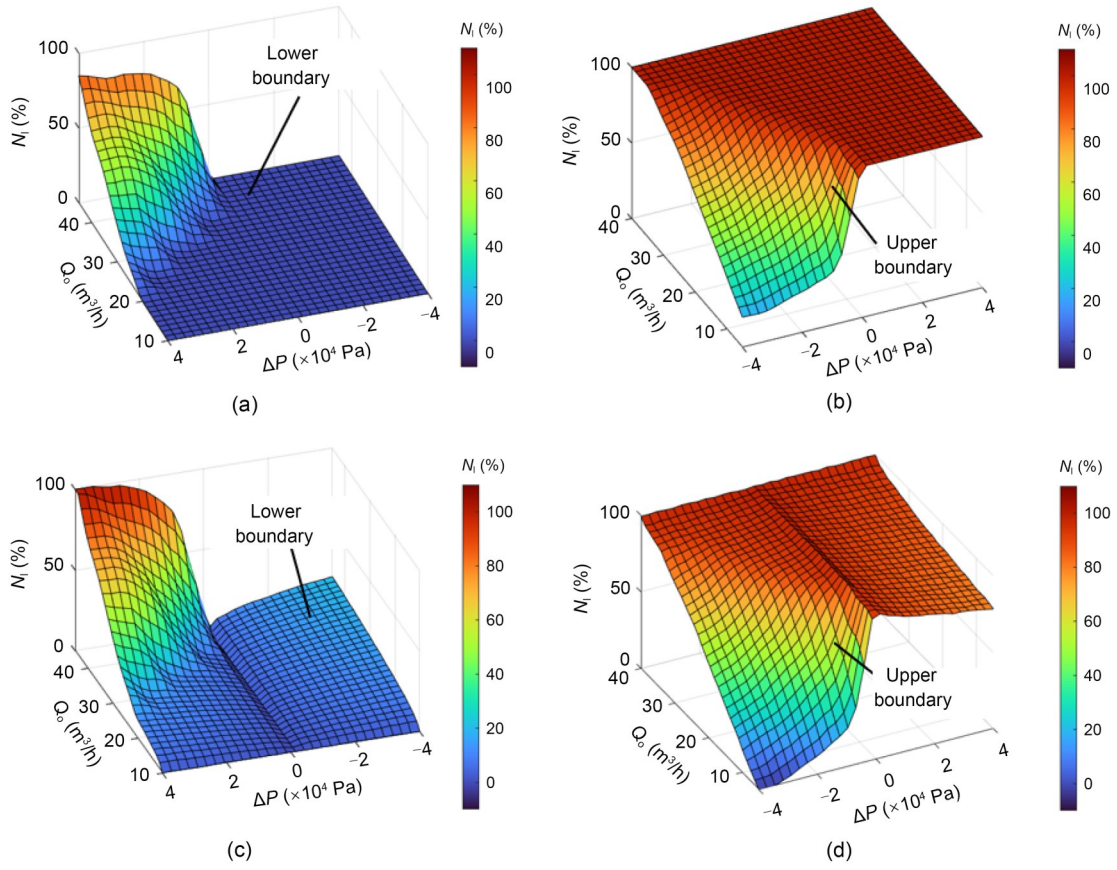

Fig. 9 Effective boundary and controllable boundary of the TCCV: (a) lower effective boundary; (b) upper effective boundary; (c) lower controllable boundary; (d) upper controllable boundary

condition. Under these operating conditions, the flow rates of the two inlets change very little when N_1 is changed. This means that changing the degree of opening has very little effect on the concentration of the outlet mixture, which seriously affects the valve's ability to control the concentration of boric acid. The controllable boundary is shown in Figs. 9c and 9d.

If a TCCV is reliable, three conditions need to be met: (1) there should be no backflow in the valve to ensure safety; (2) the operating condition should be controllable to ensure the ability to control the concentration of boric acid; (3) the local flow resistance of the valve must be less than the given value to ensure that the suction head of pumps and other equipment is sufficient.

Therefore, the ratio of the boundary volume between the effective domain and the controllable domain was taken as the parameter to evaluate the control performance of the TCCV, and this parameter was set as γ (the adjustable operating range of the TCCV). The maximum local flow resistance was used as a parameter to evaluate the flow resistance performance of the TCCV, and this parameter was set as δ. The higher the value of γ, the easier it is to satisfy conditions (1) and (2). The lower the value of δ, the easier it is to satisfy condition (3). Thus, making γ increase and δ decrease helps mitigate backflow in the TCCV. For the valve used in this study, we calculated that γ=65.1% and δ=7.82 m. Under a given operating condition, the flow in the TCCV is determined by its structure. Therefore, to make γ increase and δ decrease, the structure of the TCCV should be modified. Compared to other components in the TCCV, throttling windows have the greatest impact on flow. Therefore, in the following section, we delve deeper into optimizing the throttling windows to increase γ and decrease δ.

3.3 Throttling window optimization

Define the function $f_w(x)$ as:

$$f_w(x)=\sum_{i=0}^{3}a_i x^i, \tag{18}$$

where a_i (i=0, 1, 2, 3) is the polynomial coefficient, and a_0–a_3 range in 0–6, -5×10^{-2}–5×10^{-2}, -2.5×10^{-4}–2.5×10^{-4}, and -1.5×10^{-6}–1.5×10^{-6}, respectively. High-order coefficients were set to smaller ranges compared to low-order coefficients to avoid excessive distortion in the shape of the throttling window.

The original throttling windows had a width of 6.5 mm and a length of 74.0 mm. To ensure the throttling window area remained of the same order of magnitude during optimization, the coefficient ranges were selected accordingly. In each range of values, three points were taken at equal intervals, resulting in a total of 81 parameter combinations. Then, the γ and δ of these parameter combinations were calculated by the method used for intersection flow characteristics. The data obtained were used for quadratic regression fitting after normalization. The goodness of fit R^2 is shown in Fig. 10. The color of the points in Fig. 10 shows the deviation between the points and the line. The R^2 of both performance indexes is higher than 0.8; therefore, the fitting error is acceptable.

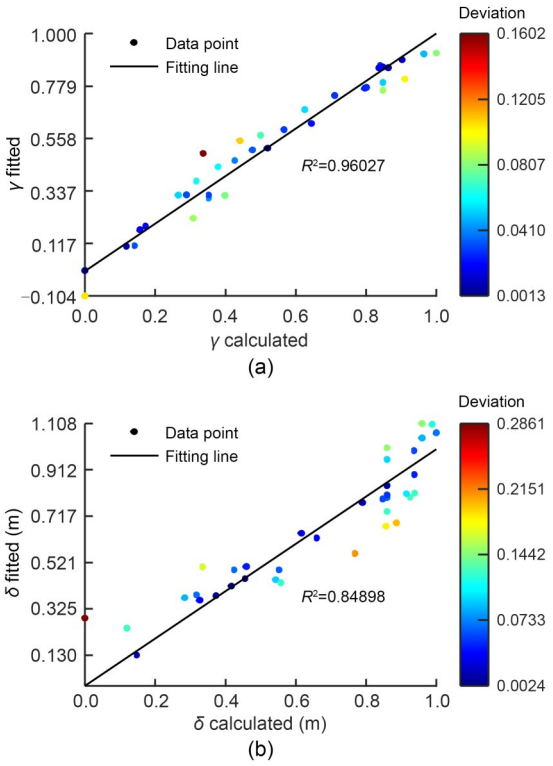

Fig. 10 Goodness of fit R^2 of two performance indexes: (a) γ; (b) δ

A series of optimal points obtained through ANSGA-II were connected to obtain the Pareto front (Fig. 11). The weight coefficients of the normalized evaluation parameters γ_{nor} and δ_{nor} were equal. The optimal curve is tangent to the straight line at (0.7230, 1.0754), which is the optimal result in the design space.

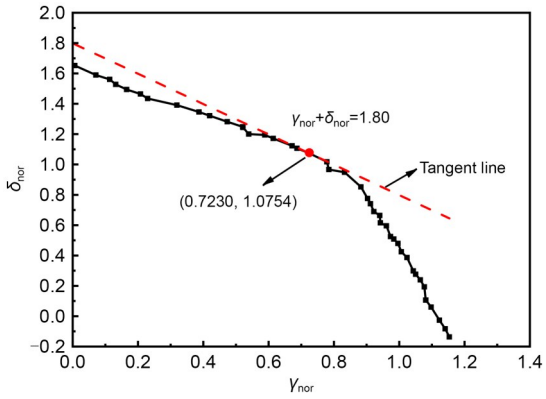

Fig. 11 Pareto front of ANSGA-II

When obtaining the optimal point, the coefficients a_0–a_3 of the throttle window function were 3.34, 3.41×10^{-2}, −1.25×10^{-4}, and −3.65×10^{-7}, respectively. Before optimization, the adjustable operating range was γ=65.1%, and the maximum local flow resistance was δ=7.82 m. After optimization, the adjustable operating range was γ=85.3%, and the maximum local resistance was δ=6.39 m. Therefore, we conclude that the adjustable operating range increased by 31.0%, and the maximum local resistance decreased by 18.3%. The flow ratio on the inlet 1 side K_{q1} and on the inlet 2 side K_{q2} of the TCCV after adopting the optimized throttling window shape were compared with the results obtained before optimization (Fig. 12). The results before optimization are experimental data, and the results after optimization are data obtained according to the proposed calculation method. After optimization, the control dead zone of the middle degree of opening has been eliminated (Fig. 12). As the degree of opening increases, the flow ratio K_{q1} on the inlet 1 side and the flow ratio K_{q2} on the inlet 2 side change approximately linearly. Therefore, we conclude that after optimization, the comprehensive performance of the TCCV has been improved. The problems of a limited adjustable operating range and excessive flow resistance under some operating conditions have been partially solved.

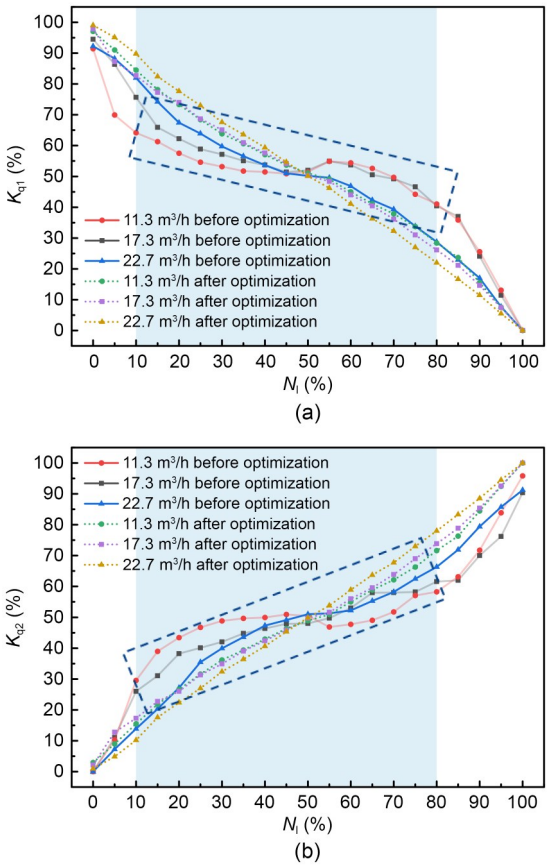

Fig. 12 Flow ratio of the TCCV before and after optimization: (a) flow ratio on the inlet 1 side K_{q1}; (b) flow ratio on the inlet 2 side K_{q2}

4 Conclusions

This paper addresses the issues of the suboptimal control performance and high flow resistance in TCCVs used in nuclear power plants for regulating boron acid concentration. The study involved the development of an experimental platform to validate a numerical model, a detailed theoretical analysis of the valve's intersection flow characteristics, and multi-objective optimization of the shape of the throttling window using the ANSGA-II. Based on the analysis, we drew the following conclusions:

(1) The flow rate distribution analysis shows that the flow rates through the left and right throttling windows vary linearly with the degree of opening, while the middle throttling windows maintain relatively constant flow rate ratios. This information is crucial for calculating the equivalent contraction ratio and assessing the valve's control performance and flow resistance.

(2) Backflow can occur when the pressure difference between the two inlets is significant. The backflow phenomenon can be divided into four stages, from no backflow to significant backflow. Defining operational boundaries ensures that the valve operates safely and effectively, maintaining the desired boric

acid concentration at the outlet without backflow. The analysis of the flow field revealed that the left throttling window is the first to experience backflow. Therefore, ensuring no backflow in the left throttling window is vital for the effectiveness of the TCCV.

(3) The optimization of the shape of the throttling window using the ANSGA-II resulted in a 31.0% increase in the adjustable operating range and an 18.3% reduction in the maximum local resistance improving the comprehensive performance of the TCCV.

These improvements offer clear benefits for nuclear power operations. Better control performance enables more precise regulation of boron acid concentration, which is essential for maintaining reactor safety and stability. This can lead to reduced downtime and lower maintenance costs associated with valve performance. Meanwhile, the reduction in flow resistance helps ensure sufficient pump head, which is critical for maintaining the stability of the system. Overall, these enhancements can improve the operational reliability of nuclear power plants, contributing to safer and more economically viable plant operations.

This study provides an approach to enhancing the design and performance of TCCVs. The methods and findings offer solutions for improving the efficiency and reliability of TCCVs in nuclear power plants. The optimized valve design can reduce maintenance costs and extend the operational lifespan of the equipment, contributing to safer and more efficient plant operations. Future work should focus on validating these findings through additional experimental testing and exploring the impact of optimized designs on other flow characteristics.

Acknowledgments

This work is supported by the National Natural Science Foundation of China (No. 52422506).

Author contributions

Jin-yuan QIAN: conceptualization, methodology, resources, validation, writing–original draft, and funding acquisition. Zhe-hui MA and Shi-jie LIN: conceptualization, investigation, methodology, data curation, writing–original draft, optimization, and visualization. Chuang LIU: conceptualization, investigation, resources, data curation, and writing–original draft. Yu-wei WANG: writing–review & editing, visualization, and project administration. Fei LING, Liang ZHANG, Man-man CUI, and Tian-zuo QU: resources and experiment. Zhi-jiang JIN: resources, writing–review & editing, visualization, project administration, and funding acquisition.

Conflict of interest

Jin-yuan QIAN, Zhe-hui MA, Shi-jie LIN, Chuang LIU, Yu-wei WANG, Fei LING, Liang ZHANG, Man-man CUI, Tian-zuo QU, and Zhi-jiang JIN declare that they have no conflict of interest.

References

Ando M, Okamoto A, Nagai H, 2023. Effect of flow resistance of floating-type check valves on heat transfer characteristics of an oscillating heat pipe. *ASME Journal of Heat and Mass Transfer*, 145(10):101004. https://doi.org/10.1115/1.4062783

Arbabi Yazdi Y, Toossian Shandiz H, Gholizadeh Narm H, 2022. Stiction detection in control valves using a support vector machine with a generalized statistical variable. *ISA Transactions*, 126:407-414. https://doi.org/10.1016/j.isatra.2021.07.020

Bao YH, Wang HG, 2022. Numerical study on flow and heat transfer characteristics of a novel Tesla valve with improved evaluation method. *International Journal of Heat and Mass Transfer*, 187:122540. https://doi.org/10.1016/j.ijheatmasstransfer.2022.122540

Blasiak S, Laski PA, Takosoglu JE, 2021. Rapid prototyping of pneumatic directional control valves. *Polymers*, 13(9): 1458. https://doi.org/10.3390/polym13091458

Brilianto RM, Seong H, Kwak H, et al., 2020. Improvement of 3-way valve for temperature control of gas turbine lube oil in CCPP. *International Journal of Precision Engineering and Manufacturing*, 21(7):1321-1332. https://doi.org/10.1007/s12541-020-00339-3

Chen FQ, Jin ZJ, 2023. Effects of perforated plate on hydrogen flow in L-shaped high pressure reducing valve. *International Journal of Hydrogen Energy*, 48(5):1956-1967. https://doi.org/10.1016/j.ijhydene.2022.09.276

Cui WL, Wang DX, Hong X, et al., 2024. Research and development of innovative bidirectional control plate valve for reciprocating compressor. *Applied Energy*, 365:123279. https://doi.org/10.1016/j.apenergy.2024.123279

Filho LSC, Filho JGD, Vatavuk P, et al., 2023. A new model of hydraulic valve for building installations which has a sliding command and which works completely embedded in the masonry. *Water*, 15(8):1441. https://doi.org/10.3390/w15081441

Filo G, Lisowski E, Rajda J, 2021. Design and flow analysis of an adjustable check valve by means of CFD method. *Energies*, 14(8):2237. https://doi.org/10.3390/en14082237

Guan AQ, Xu JX, Jin ZJ, et al., 2023. Damping effect and fluid dynamic analysis on closing process of axial flow check valve. *Journal of Fluids Engineering*, 145(10):101204. https://doi.org/10.1115/1.4062822

Guan AQ, Xiang FN, Lin ZH, et al., 2024. Experimental and modeling investigation on dynamic response of sticky control valves. *Control Engineering Practice*, 148:105953. https://doi.org/10.1016/j.conengprac.2024.105953

Gui SY, Zhang SS, Fu B, et al., 2022. Fluid-dynamic analysis

and multi-objective design optimization of piezoelectric servo valves. *Flow Measurement and Instrumentation*, 85: 102157. https://doi.org/10.1016/j.flowmeasinst.2022.102157

Guo QS, Wu X, Cai H, et al., 2024. Multi-power sources joint optimal scheduling model considering nuclear power peak regulation. *Energy*, 293:130678. https://doi.org/10.1016/j.energy.2024.130678

Hadebe XP, Tchomeni Kouejou BX, Alugongo AA, et al., 2024. Finite element analysis and computational fluid dynamics for the flow control of a non-return multi-door reflux valve. *Fluids*, 9(10):238. https://doi.org/10.3390/fluids9100238

Haneklaus N, Qvist S, Gładysz P, et al., 2023. Why coal-fired power plants should get nuclear-ready. *Energy*, 280:128169. https://doi.org/10.1016/j.energy.2023.128169

Hopfgartner J, Almbauer R, Egger A, et al., 2022. Investigation of force-assisted suction reed valves in hermetic reciprocating compressors. *Proceedings of the Institution of Mechanical Engineers, Part E: Journal of Process Mechanical Engineering*, 236(1):26-35. https://doi.org/10.1177/0954408918818739

Hu H, Son I, Kikumoto H, et al., 2024. Improving Tesla valve shape within fluid diode plates for building ventilation. *Building and Environment*, 252:111259. https://doi.org/10.1016/j.buildenv.2024.111259

Kang HL, Park HJ, Han SH, 2024. Evaluation of cavitation phenomena in three-way globe valve through computational analysis and visualization test. *Scientific Reports*, 14(1):21919. https://doi.org/10.1038/s41598-024-72585-8

Lin ZH, Li JY, Jin ZJ, et al., 2021. Fluid dynamic analysis of liquefied natural gas flow through a cryogenic ball valve in liquefied natural gas receiving stations. *Energy*, 226: 120376. https://doi.org/10.1016/j.energy.2021.120376

Lisowski E, Filo G, Pluskowski P, et al., 2023. Flow analysis of a novel, three-way cartridge flow control valve. *Applied Sciences*, 13(6):3719. https://doi.org/10.3390/app13063719

Lisowski E, Filo G, Rajda J, 2024. Adjustment of proportional control valve characteristics via pressure compensation using flow forces. *Energies*, 17(7):1546. https://doi.org/10.3390/en17071546

Mallapaty S, 2020. How China could be carbon neutral by mid-century. *Nature*, 586(7830):482-483. https://doi.org/10.1038/d41586-020-02927-9

Qian JY, Hou CW, Mu J, et al., 2020. Valve core shapes analysis on flux through control valves in nuclear power plants. *Nuclear Engineering and Technology*, 52(10):2173-2182. https://doi.org/10.1016/j.net.2020.03.008

Qian JY, Wu W, Cheng M, et al., 2022. Practice of flow control and smart valves. *Journal of Zhejiang University-SCIENCE A*, 23(4):243-246. https://doi.org/10.1631/jzus.A22FCSV1

Rajesh P, Toley M, Mal D, et al., 2024. Impact of adding high-concentration neutron poisons to reactor moderator system for guaranteed shutdown. *Progress in Nuclear Energy*, 176:105397. https://doi.org/10.1016/j.pnucene.2024.105397

Singh D, Aliyu AM, Charlton M, et al., 2020. Local multiphase flow characteristics of a severe-service control valve. *Journal of Petroleum Science and Engineering*, 195: 107557. https://doi.org/10.1016/j.petrol.2020.107557

Vašina M, Hružík L, Bureček A, et al., 2015. Dynamical behaviour of three-way throttle valve with pressure gradient stabilization. *EPJ Web of Conferences*, 92:02104. https://doi.org/10.1051/epjconf/20159202104

Wang HW, Nan LJ, Zhou X, et al., 2024. Research on noise reduction of water hydraulic throttle valve based on RBF neural network and multi-island genetic algorithm. *Machines*, 12(5):333. https://doi.org/10.3390/machines12050333

Witrant E, Landau ID, Vaillant MP, 2023. A data-driven control methodology applied to throttle valves. *Control Engineering Practice*, 139:105634. https://doi.org/10.1016/j.conengprac.2023.105634

Yang MK, Zhang YH, Ai C, et al., 2023. Multi-objective optimisation of K-shape notch multi-way spool valve using CFD analysis, discharge area parameter model, and NSGA-II algorithm. *Engineering Applications of Computational Fluid Mechanics*, 17(1):2242721. https://doi.org/10.1080/19942060.2023.2242721

Zhao GC, Zhou GQ, Wang H, et al., 2023. Groove parameters optimization of rotary excitation control valve using computational fluid dynamics coupled with response surface method. *Ain Shams Engineering Journal*, 14(12):102575. https://doi.org/10.1016/j.asej.2023.102575

Zong CY, Li QY, Li KP, et al., 2022a. Computational fluid dynamics analysis and extended adaptive hybrid functions model-based design optimization of an explosion-proof safety valve. *Engineering Applications of Computational Fluid Mechanics*, 16(1):296-315. https://doi.org/10.1080/19942060.2021.2010602

Zong CY, Shi ML, Li QY, et al., 2022b. Design optimization of a nuclear main steam safety valve based on an E-AHF ensemble surrogate model. *Nuclear Engineering and Technology*, 54(11):4181-4194. https://doi.org/10.1016/j.net.2022.06.019